Geogrid-stabilized eco-friendly aggregates for pavement base – quantitative assessment using Bender Element sensor technology

Han Wang[1], *Hyojung* Ko[1], *Mingu* Kang[2], *Erol* Tutumluer[3*], and *Heather* Shoup[4]

[1]Graduate Research Assistant, University of Illinois Urbana-Champaign, IL 61801, USA
[2]Assistant Professor, University of St. Thomas, St. Paul, MN 55105, USA
[3]Abel Bliss Professor, University of Illinois Urbana Champaign, IL 61801, USA
[4]Central Office Geotechnical Engineer, Illinois Dept. of Transportation, Springfield IL 62704, USA

Abstract. Geogrids provide mechanical stabilization by effectively restraining aggregate movements in a granular layer which in turn improve pavement performance and extend its lifespan. This paper presents an experimental evaluation of a multi-axial extruded geogrid stabilizing two types of eco-friendly aggregates, i.e., virgin crushed limestone and recycled concrete aggregate, used in pavement unbound base/subbase applications. The study evaluated geogrid stabilized aggregate resilient modulus and permanent deformation characteristics and assessed the modulus enhancement provided by the geogrid. Repeated load triaxial tests were conducted on 152-mm (6-in.) diameter and 305-mm (12-in.) high cylindrical specimens, instrumented with embedded Bender Element (BE) shear wave transducers. Both control specimens and geogrid-stabilized specimens with geogrid placed at specimen midheight were constructed. During resilient modulus testing, shear wave velocity measurements were also taken by the transmitter-receiver BE sensor pairs embedded immediately above the specimen midheight to determine small-strain moduli. Specimen permanent deformations were then evaluated for up to 10,000 load repetitions. The geogrid-stabilized specimens had lower permanent deformations than the control specimens and provided considerable local stiffness enhancements for both the recycled and natural aggregates to demonstrate a sustainable geosynthetic application.

1 Introduction

Geogrids improve paved and unpaved road performance by mechanically stabilizing an unbound aggregate base or subbase course. The inclusion of geogrid can help reduce required aggregate layer thickness or extend pavement lifespan given the same traffic conditions. Among many available geogrids on the market, extruded geogrids are the most common types, with which aggregate particle lateral movements can be restricted by aggregate particle strikethrough in the apertures thus providing an effective “interlocking” mechanism [1].

* Corresponding author: tutumlue@illinois.edu

Since the introduction of geotextiles and geogrids to roadway applications, various methods to incorporate these geosynthetics into pavement construction have been proposed including soft subgrade stabilization approaches by Steward et al. (1978) method [2], Giroud and Noiray (1981) method [3]. Dutch (CROW) method [4], US Army Corps of Engineers (ERDC) method [5], Giroud and Han (2004) method [6], etc. These pavement working platform or unpaved road design methods mainly formulate a solution for general bearing capacity failure since the use of geosynthetic is intended to effectively avoid a punching shear failure on soft subgrade. The quantitative evaluation of a geosynthetic product, preferably a geogrid, in mechanical stabilization should consider what is known as the lateral restraint mechanism for effectively restricting aggregate particle movements. Meanwhile, the method should provide repeatable assessment mechanically stabilized layer inputs for mechanistic-empirical pavement design procedures (MEPDG) [7]. Recently, two evaluation methods that deal with interaction properties, i.e., soil-geosynthetic composite stiffness (K_{SGC}) and small strain modulus measurement via Bender Element (BE) shear wave transducers, have been proposed to quantitatively assess a geogrid's effectiveness in mechanical stabilization [8–11].

Other than geogrids, which offer a sustainable engineered solution to permanent pavement foundation designs, the use of recycled materials has also been promoted to reduce the consumption of energy and greenhouse gas emissions along with virgin aggregate production. Recycled concrete aggregates (RCA) are one of the recycled materials, deemed to have comparable characteristics as virgin aggregates [12]. In this study, both a virgin crushed limestone (CL) and RCA were evaluated in terms of their resilient modulus and permanent deformation characteristics in laboratory repeated load triaxial testing. In addition, small-strain shear moduli were determined from shear wave velocity measurements using a source-receiver type BE shear wave transducers embedded in the triaxial samples. To assess how the geogrid inclusion could improve aggregate response and performance trends, five specimens, i.e., one CL specimen without geogrid and one CL specimen with geogrid, and two RCA specimens without geogrid and one RCA specimen with geogrid, were tested using the repeated load triaxial test setup. The trend of geogrid-stabilized specimens exhibiting lower permanent deformations than the control specimens were in line with the local stiffness enhancements observed for both the recycled and natural aggregates.

2 Material and method

2.1 Material

2.1.1 Crushed limestone (CL) and recycled concrete aggregate (RCA)

Virgin CL and RCA utilized for this study were obtained from local quarries and construction sites in Illinois, USA. The gradations of both aggregates were obtained as per ASTM C136 and conformed to Illinois Department of Transportation (IDOT) CA 6 dense-graded aggregate gradation band. The gradations are presented in ***Fig. 1***, and all specimens used in this study were engineered to follow the specific gradations for consistency.

As per ASTM C127, the specific gravities of both aggregates were determined and presented in **Table 1**. Under the standard Proctor compaction effort as per ASTM D698, the maximum dry density (MDD) and optimum moisture content (OMC) for both aggregates were also determined, as presented in **Table 1**. Note that although two aggregates follow similar gradation, RCA has a higher OMC and lower MDD when compared to virgin CL. On one hand, the RCA material has lower specific gravity and the hydration and cementation of unhydrated cement particles may lead to a lower MDD. On the other hand, RCA tend to exhibit hydrophilic properties due to the presence of porous residual mortar within their

structure, which increases OMC [12]. To evaluate aggregate performance trends at a lower compactive effort, i.e., more eco-friendly, specimens were constructed at target densities at around 95% of MDD. All control and geogrid (GG) stabilized specimen achieved densities are reported in **Table 1**.

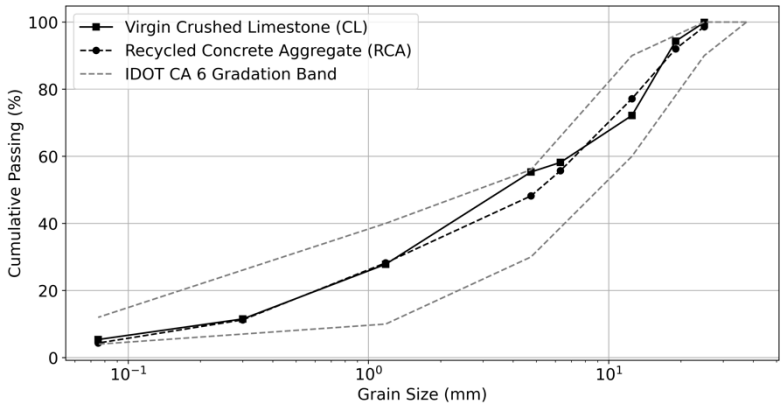

Fig. 1. Particle size distributions of aggregate materials and the IDOT CA 6 gradation band

Table 1. Aggregate physical properties and achieved specimen densities.

	Specific Gravity (ASTM C127)	MDD (ASTM D698)	OMC (ASTM D698)	Achieved Specimen Density (Percent compaction)
CL	2.70	21.9 kN/m^3	6.7%	Control 1 – 21.2 kN/m^3 (97%) GG 1 – 21.2 kN/m^3 (97%)
RCA	2.61	18.9 kN/m^3	12.8%	Control 1 – 18.5 kN/m^3 (98%) Control 2 – 18.3 kN/m^3 (97%) GG 1 – 18.1 kN/m^3 (96%)

The morphological properties of the virgin CL and RCA were evaluated using the Enhanced University of Illinois Aggregate Image Analyzer (E-UIAIA). Imaging based morphological indices including angularity index (AI), flat and elongated (F&E) ratio and surface texture (ST) were quantified based on three orthogonal views of each particle [13]. The average index values along with the standard deviations (shown as error bars) from two duplicate tests of more than 50 particles retained on each sieve size are presented in ***Fig. 2***.

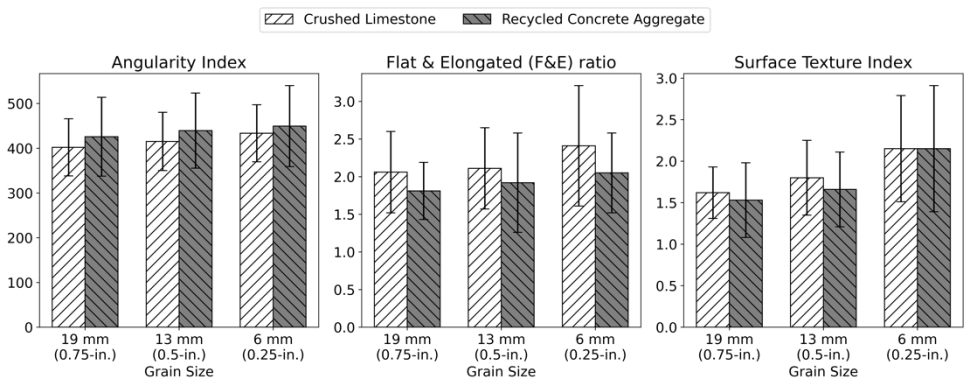

Fig. 2. Imaging based morphological indices of crushed limestone and recycled concrete aggregate.

In general, RCA has a slightly higher AI as compared to virgin CL, which is expected given that RCA agglomerations typically have adhered mortar [14, 15]. Virgin CL has higher F&E ratio, which may make it more susceptible to chipping and breakage. RCA particles are also expected to have rougher surface (i.e., higher ST index) than virgin aggregates [14]. Yet, in this study, for 19 mm and 13 mm particles, RCA have slightly lower ST index while for 6 mm particles, RCA and CL have comparable ST indices.

2.1.2 Multi-axial Geogrid

The multi-axial geogrid used in this study was manufactured from a coextruded composite polypropylene (PP) sheet, which was then punched, oriented, and stretched to form desired aperture geometry. Three different aperture shapes are present including hexagons, trapezoids, and triangles. The geogrid coupon tested in triaxial tests is shown in **Table 2**. The coupon includes all three aperture geometries while keeping a symmetric structure. Rib thickness, rib width and rib pitch and the inscribed circle diameter in each aperture are also noted in **Table 2**.

Table 2. Multi-axial punched and drawn geogrid properties.

Geogrid Coupon	Polymer type	Geogrid Type	Rib Thickness	Rib Width	Rib Pitch	Diameter of Largest Inscribed Circle, A_{min}
			mm	mm	mm	mm
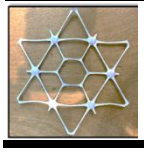	Polypropylene (PP)	Extruded	2.50	1.50	80 Between parallel ribs	34.6 (Hexagon) 22.7 (Trapezoid) 26.7 (Triangle)

2.2 Experimental Method

The TX-12 triaxial test setup at the University of Illinois was utilized in this study, which can accommodate a cylindrical specimen 152 mm (6 in.) in diameter and 305 mm (12 in.) in height. The cell confining pressure was applied through pressured air inside the acrylic chamber and the repeated load pulses, which simulate wheel load passes, were applied through a hydraulic pump and measured by the load cell placed on specimen top. The vertical deformation was measured through two internal linear variable differential transformers (LVDTs) placed inside the acrylic chamber. For geogrid-stabilized specimens, the geogrid coupons were placed at specimen midheight. Three pairs of BE sensors were placed at three different heights above specimen midheight to assess the local small-strain shear modulus. A schematic drawing and a photo showing the setup are given in ***Fig. 3***.

2.2.1 Resilient modulus test

The resilient modulus test was conducted in accordance with AASHTO T307 test procedure. The resilient moduli of granular aggregate specimens were evaluated at 15 different loading stages, following a conditioning stage. The 15 loading stages consist of three deviator stresses pulsed at each of five different confining pressures [i.e., 20.7 kPa (3 psi), 34.5 kPa (5 psi), 68.9 kPa (10 psi), 103.4 kPa (15 psi) and 137.9 kPa (20 psi)]. In each load stage, 100 haversine pulses, i.e., 100-ms loading and 900-ms rest periods, were applied.

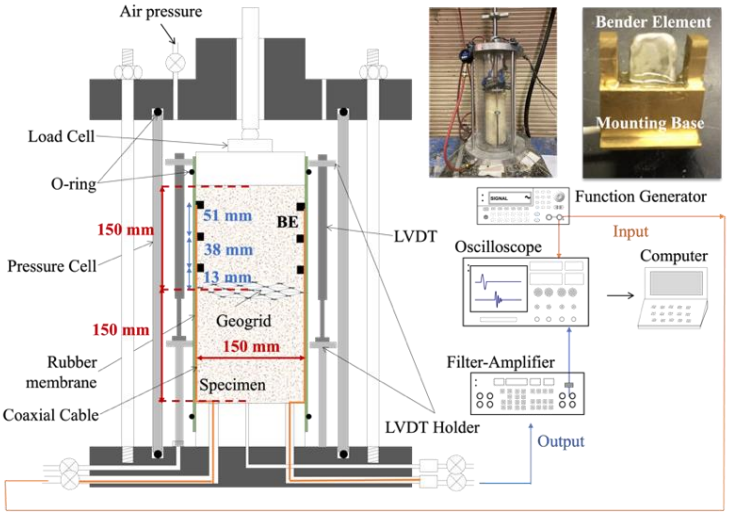

Fig. 3. Triaxial test setup showing embedded Bender Element (BE) sensor pairs at three heights.

2.2.2 Permanent deformation test

After the conditioning and 15 load stages as specified in the AASHTO T307 procedure, additional 10,000 load pulses were applied to aggregate specimens further evaluate their permanent deformation accumulation trends at a deviator stress of 413.7 kPa (60 psi) and a confining pressure of 137.9 kPa (20 psi). Each haversine pulse consisted of 100-ms loading and 900-ms rest periods. The selection of deviator stress and confining pressure aimed to introduce an applied stress ratio (σ_1/σ_3) of 4, which is typical for permanent deformation evaluation while not introducing any stress history influence since the maximum deviator stress and confining pressure values achieved before the permanent deformation test were 275.8 kPa (40 psi) and 137.9 kPa (20 psi) [16].

2.2.3 Small-strain shear modulus from Bender Element sensors

The small-strain shear modulus was assessed through pairs of BE sensors embedded at two ends of the specimens, as shown in **Fig. *3***. The signal generator excited the source BE sensor to transmit shear waves through the aggregate specimen and the arriving shear waves were measured by the receiver BE sensor at the other end. Before finalizing shear wave velocity measurements, the signals were filtered, amplified, stacked, and averaged for obtaining a clear signal with higher signal to noise ratio (SNR).

3 Results and discussion

3.1 Resilient modulus

Resilient modulus M_r is determined as the ratio of the applied deviator stress to axial recoverable strain and averaged from the last five load repetitions at each load stage, as given in Equation 1.

$$M_r = \frac{\sigma_d}{\varepsilon} \quad (1)$$

where σ_d is the deviator stress and ε is the axial recoverable strain. The resilient moduli determined for each specimen are presented in **Fig. *4***. Unbound aggregate materials exhibit stress-hardening characteristics, which can be characterized using a K-Theta model, where a power function is established between resilient modulus and applied bulk stress [17]. The K-Theta models developed from regression analyses of the test data along with the coefficients of determination (R^2) for all tests are presented in **Fig. *4***.

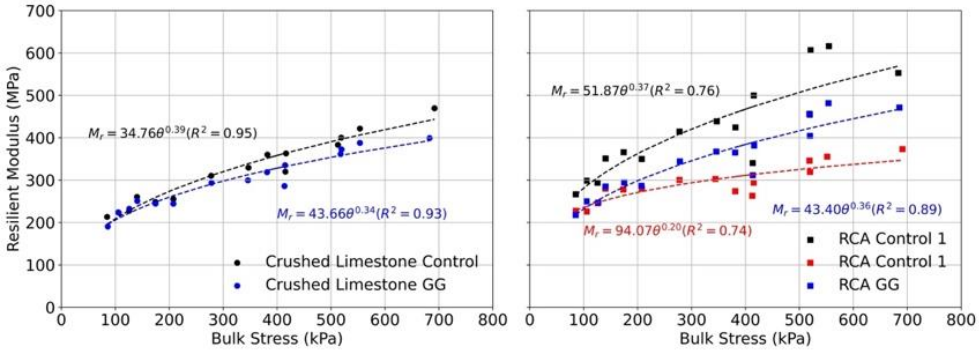

Fig. 4. Resilient moduli determined for all specimens tested and K-Theta models developed.

Virgin CL resilient modulus trends exhibited high R^2 values for both tests which are typical for dense-graded granular materials. On the other hand, resilient moduli of RCA exhibited relatively lower R^2 values, with which the moduli also showed large variation as compared to virgin CL. On one hand, the higher variability in resilient moduli for RCA may be due to the fact that recycled materials were possibly obtained from different sources [18]. On the other hand, the lower R^2 value may indicate RCA resilient moduli are more variable and do not follow consistent load-deformation behavior as well as virgin unbound aggregates due to the existence of mortar. Yet, for both aggregates, the inclusion of geogrid did not lead to an improvement in resilient modulus. Similar observations were reported by previous researchers, where it was concluded that the influence of geogrids should be evaluated through other ways [11, 19–22].

3.2 Permanent deformation

The permanent deformation (PD) or cumulative strain was evaluated through three phases including: (a) conditioning stage, where deviator stress and confining pressure were both 103.4 kPa (15 psi); (b) 15 different loading stages at various deviator stress and confining pressure levels as specified in AASHTO T307; and (c) the final PD test, where load pulses with deviator stress at 413.7 kPa (60 psi) and confining pressure was set to 137.9 kPa (20 psi). The accumulated strain values from three phases are presented in ***Fig. 5*** (a), (b) and (c).

From the conditioning stage, geogrid-stabilized specimens showed a better performance given less cumulative strain for both aggregates. Further, during the 15 loading stages and the final PD test, geogrid-stabilized specimens consistently exhibited lower cumulative strains, which showed geogrid's effect in improving PD accumulation. Note that after the conditioning stage, less variation is observed between two RCA control test results thus indicating an evaluation after the conditioning stage is necessary given that possible structure variation during compaction and the specimen shakedown has been compensated during the conditioning stage. The cumulative strains and improvements with geogrid inclusion are presented in **Table 3**. Note that after the conditioning stage, RCA specimens exhibited lower permanent strain accumulations as compared to virgin CL, which may be due to a higher angularity of RCA which helped achieve better interlocking and shakedown of aggregates.

(a)	Cumulative strain during conditioning stage $\sigma_d = \sigma_c = 103.4\ kPa$ $(15\ psi)$	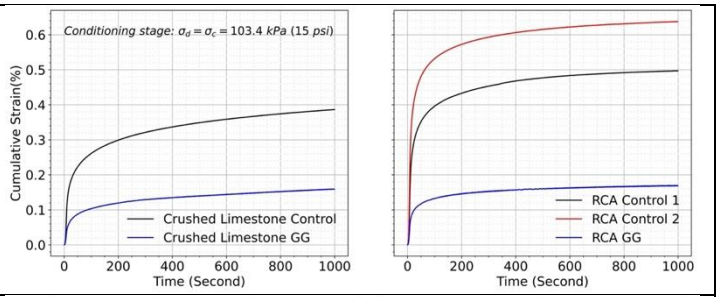
(b)	Cumulative strain during AASHTO T307 15 loading stages	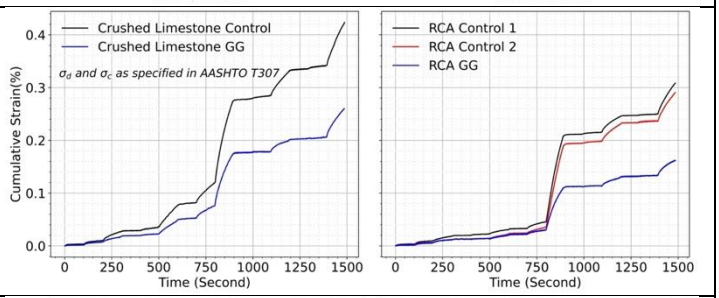
(c)	Cumulative strain during permanent deformation test $\sigma_d = 413.7\ kPa$ $(60\ psi)$ $\sigma_c = 137.9\ kPa$ $(20\ psi)$	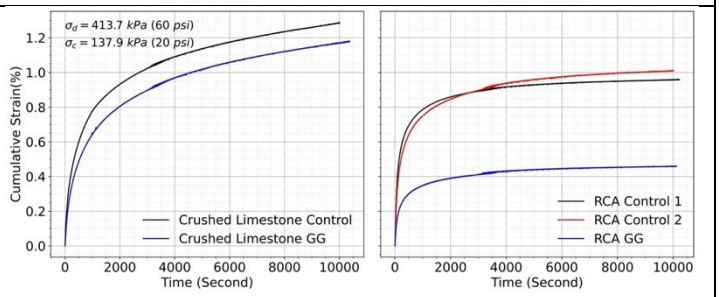

Fig. 5. Cumulative strains recorded as indicators of permanent deformation accumulation during three loading stages.

Table 3. Cumulative strain comparison during three loading stages.

Cumulative strain (%)		Conditioning stage	15 loading stages	Final PD test
CL	**Control**	0.39	0.42	1.28
	GG	0.16 **(-59.0%)**	0.26 **(-38.1%)**	1.18 **(-7.8%)**
RCA	**Control Avg.**	0.57	0.30	0.98
	GG	0.17 **(-70.2%)**	0.16 **(-46.7%)**	0.46 **(-53.1%)**

3.3 Small-strain shear modulus

The small-strain shear modulus can be determined using Equation 2.

$$G_{BE} = \rho V_s^2 = \rho\left(\frac{L_{tip-to-tip}}{t}\right)^2 \quad (2)$$

where G_{BE} is small-strain shear modulus, ρ is specimen's bulk density, V_s is shear wave velocity, $L_{tip-to-tip}$ is the tip to tip distance between BE source and receiver, and t is the first

arrival time determined from collected shear wave signals. Each signal was collected when the confining pressure was maintained without any applied deviator stress. Under the same confining pressure, the specimens did not undergo any large deformation or skeleton shift, which led to similar signals and first arrival times. Therefore, a representative average modulus from three measurements under the same confining pressure was calculated. The measured G_{BE} right above specimen midheight or geogrid location, along with the well-established regression model between G_{BE} and confining pressure is presented in ***Fig. 6***.

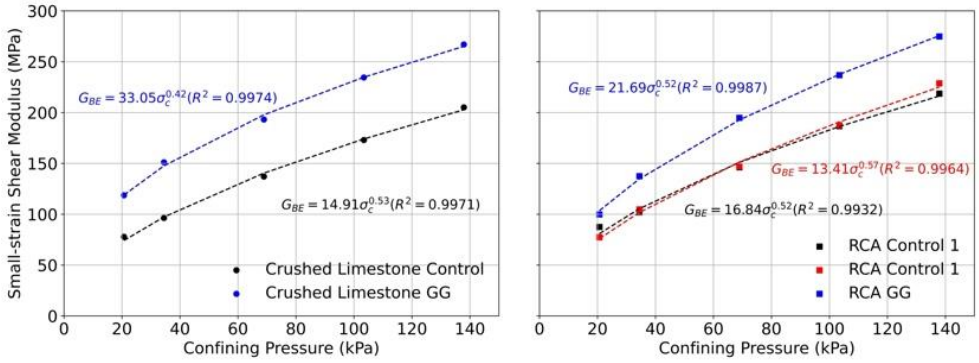

Fig. 6. Small-strain shear moduli computed at 13 mm (0.5 in.) above specimen midheight/GG.

Right above the geogrid, i.e., 13 mm (0.5 in.) above the geogrid, higher G_{BE} values were computed for both aggregates when compared to those of the control specimens without geogrid. The G_{BE} along with enhancement values determined at different confining pressures are presented in **Table 4**. The BE sensor pairs adequately measured shear wave velocities to compute these quantitative modulus enhancement values, which can be converted to resilient modulus improvements at larger strain levels and incorporated into Mechanistic-Empirical (ME) pavement design procedures. Note that three pairs of BE sensors have been installed to assess different modulus enhancement levels at various distances from geogrid to adequately characterize the mechanically stabilized layer. Such assessments of both modulus enhancement and extent of geogrid influence zone will further help incorporate influences of various geogrids into ME pavement design procedures.

Table 4. Small-strain shear modulus comparison.

Confining pressure (kPa)		20.7	34.5	68.9	103.4	137.9	Overall
CL G_{BE} (MPa)	Control	77.80	96.35	137.06	173.02	205.11	-
	GG	118.63 **(+52%)**	151.05 **(+57%)**	193.17 **(+41%)**	234.48 **(+36%)**	266.98 **(+30%)**	**+43%**
RCA G_{BE} (MPa)	Control Avg.	82.41	103.35	146.60	187.17	223.70	-
	GG	99.82 **(+21%)**	137.47 **(+33%)**	194.82 **(+33%)**	236.81 **(+27%)**	274.86 **(+23%)**	**+27%**

4 Conclusions

In this study, both virgin crushed limestone (CL) and recycled concrete aggregate (RCA) materials were evaluated for resilient modulus and permanent deformation (PD) characteristics. Small-strain shear moduli were also studied as obtained from shear wave velocity measurements using Bender Element (BE) shear wave transducers in a laboratory

triaxial test setup. For both aggregates, the inclusion of a geogrid at specimen midheight did not improve resilient modulus but provided adequate resistance to permanent deformation/strain accumulation. Further, the BE sensors embedded in the specimens successfully quantified a local modulus enhancement, i.e., stiffening, near geogrid. The evaluation herein demonstrated the improvement from geogrid for both aggregates through reduced cumulative strain and higher local modulus, illustrating the good potential for sustainable engineered solutions for pavement construction with geosynthetics and eco-friendly aggregates.

Acknowledgments

This publication is part of the ongoing Illinois Center for Transportation (ICT) ICT-R27-234 project. The contents of this paper reflect the views of the authors, who are responsible for the facts and the accuracy of the data presented herein. The contents do not necessarily reflect the official views or policies of the ICT, the IDOT, or the FHWA. This paper does not constitute a standard, specification, or regulation. Test data are available upon request.

References

1. J. P. Giroud, J. Han, E. Tutumluer and M.J.D Dobie, The use of geosynthetics in roads. Geosynthetics International **30**, 47–80 (2023) https://doi.org/10.1680/jgein.21.00046
2. J.E. Steward, R. Williamson and J. Mohney, Guidelines for use of fabrics in construction and maintenance of low-volume roads. USDA, Forest Service (1978)
3. J.-P. Giroud and L. Noiray, Geotextile-reinforced unpaved road design. J. of the Geotech. Engineering Div. **107**, 9 (1981)
4. C.A.P.M Van Gurp, A.J van Leest, Thin asphalt pavements on soft soil. In: International Society for Asphalt Pavement, Ninth International Conference on Asphalt Pavements (2002)
5. J.S. Tingle, S.L. Webster, Corps of Engineers design of geosynthetic-reinforced unpaved roads. Transportation Research Record **1849**, 193–201 (2003) https://doi.org/10.3141/1849-21
6. J.P. Giroud, J. Han, Design method for geogrid-reinforced unpaved roads. I. Development of design method. J. Geotech. Geoenviron. Eng. **130**, 775–786 (2004) https://doi.org/10.1061/(ASCE)1090-0241(2004)130:8(775)
7. J.G. Zornberg, Advances in the use of geosynthetics in pavement design. In Proc. of the Second National Conference on Geosynthetics, Geosynthetics India '11, India Institute of Technology Madras, Chennai, India, pp. 3–21 (2011)
8. Y.-H. Byun, I.I.A. Qamhia, M. Kang, E. Tutumluer, and M.H Wayne, Modeling geogrid-stabilized aggregate base courses considering local stiffness enhancement. Geosynthetics International. 1–10 (2023). https://doi.org/10.1680/jgein.23.00086
9. J.G. Zornberg, G.H. Roodi and R. Gupta, Stiffness of soil–geosynthetic composite under small displacements: I. Model development. J. Geotech. Geoenviron. Eng. **143**, 04017075 (2017). https://doi.org/10.1061/(ASCE)GT.1943-5606.0001768

10. G.H Roodi, J.G. Zornberg, Stiffness of soil-geosynthetic composite under small displacements. II: Experimental evaluation. J. Geotech. Geoenviron. Eng. **143**, 04017076 (2017). https://doi.org/10.1061/(ASCE)GT.1943-5606.0001769
11. Y.-H. Byun, E. Tutumluer, B. Feng, J.H. Kim and M.H.Wayne, Horizontal stiffness evaluation of geogrid-stabilized aggregate using shear wave transducers. Geotextiles and Geomembranes **47**, 177–186 (2019). https://doi.org/10.1016/j.geotexmem.2018.12.015
12. B. Cetin, I. Gheibi, T.B. Edil, M. Hatipoglu and H.S. Coban, Improve material inputs into mechanistic design properties for reclaimed HMA & Recycled Concrete Aggregate (RCA) roadways. Minnesota Department of Transportation (2021)
13. M. Moaveni, S. Wang, J.M. Hart, E. Tutumluer and N. Ahuja, Evaluation of aggregate size and shape by means of segmentation techniques and aggregate image processing algorithms. Transportation Research Record **2335**, 50–59. https://doi.org/10.3141/2335-06
14. J. Andal, M. Shehata and P. Zacarias, Properties of concrete containing recycled concrete aggregate of preserved quality. Construction and Building Materials **125**, 842–855 (2016). https://doi.org/10.1016/j.conbuildmat.2016.08.110
15. A. Dawson, Alternative and recycled materials for earth construction. In: Modern Earth Buildings. pp. 172–203. Elsevier (2012)
16. I. Kim, J. Kwon, E. Tutumluer, Rutting of airport pavement granular layers. In: Airfield Pavements: Challenges and New Technologies. pp. 334–347 (2004)
17. R.G. Hicks, C.L. Monismith, Factors influencing the resilient response of granular materials. Highway Research Record. 15–31 (1971)
18. J.F. Lamond, Sr R.L Campbell., A. Giraldi, N.J.T Jenkins, T.R. Campbell, W. Halczak, R. Miller, J.A. Cazares, H.C. Hale Jr. and P.T. Seabrook, Removal and reuse of hardened concrete. American Concrete Institute, Farmington Hills, MI, USA, 26. (2001)
19. H. Wang, M. Kang, Y. Kim, I.I.A. Qamhia, E. Tutumluer and H. Shoup, Geosynthetic-stabilized aggregate: quantitative modulus evaluation via Bender Element. Geosynthetics International (2024). https://doi.org/10.1680/jgein.24.00078
20. M. Abu-Farsakh, G. Souci, G.Z. Voyiadjis and Q. Chen, Evaluation of factors affecting the performance of geogrid-reinforced granular base material using repeated load triaxial tests. J. Mater. Civ. Eng. **24**, 72–83 (2012). https://doi.org/10.1061/(ASCE)MT.1943-5533.0000349
21. M. Kang, J.H. Kim, I.I.A. Qamhia, E. Tutumluer and M.H.Wayne, Geogrid stabilization of unbound aggregates evaluated through Bender Element shear wave measurement in repeated load triaxial testing. Transportation Research Record **2674**, 113–125 (2020). https://doi.org/10.1177/0361198120908230
22. H. Wang, M. Kang, I.I.A. Qamhia, E. Tutumluer, M.H. Wayne and H. Shoup, Evaluation of open-graded aggregates stabilized with a multi-axial geogrid using a large-scale triaxial test set-up. Transportation Research Record, Journal of the Transportation Research Board **2677**, 339–350 (2023) https://doi.org/10.1177/03611981231161351